RSC
Medicinal Chemistry

ROYAL SOCIETY OF CHEMISTRY

RESEARCH ARTICLE

View Article Online
View Journal

Cite this: DOI: 10.1039/d4md00057a

Synthesis, biological evaluation and metadynamics simulations of novel *N*-methyl β-sheet breaker peptides as inhibitors of Alzheimer's β-amyloid fibrillogenesis†

Federica Moraca, ‡[ab] Ilaria Vespoli,‡[c] Domenico Mastroianni,[d] Vincenzo Piscopo,[e] Rosa Gaglione,[df] Angela Arciello,[df] Mauro De Nisco, *[g] Severina Pacifico,[e] Bruno Catalanotti [a] and Silvana Pedatella [d]

Received 22nd January 2024,
Accepted 7th April 2024

DOI: 10.1039/d4md00057a

rsc.li/medchem

Several scientific evidences report that a central role in the pathogenesis of Alzheimer's disease is played by the deposition of insoluble aggregates of β-amyloid proteins in the brain. Because Aβ is self-assembling, one possible design strategy is to inhibit the aggregation of Aβ peptides using short peptide fragments homologous to the full-length wild-type Aβ protein. In the past years, several studies have reported on the synthesis of some short synthetic peptides called β-sheet breaker peptides (BSBPs). Herein, we present the synthesis of novel (cell-permeable) *N*-methyl BSBPs, designed based on literature information on the structural key features of BSBPs. Three-dimensional GRID-based pharmacophore peptide screening combined with PT-WTE metadynamics was performed to support the results of the design and microwave-assisted synthesis of peptides **2** and **3** prepared and analyzed for their fibrillogenesis inhibition activity and cytotoxicity. An HR-MS-based cell metabolomic approach highlighted their cell permeability properties.

Introduction

Alzheimer's disease (AD) is a neurodegenerative disorder characterized by the loss of cognitive functions and dementia. Although AD etiology and pathogenesis remain rather unclear,[1] a leading theory points to progressive and massive deposits in the brain of senile plaques consisting of insoluble protein aggregates, whose main constituent is the β-amyloid protein (Aβ). Aβ is a peptide of 39 to 43 residues, produced from the amyloid precursor protein (APP) *via* the proteolytic activities of β- and γ-secretases[2] and/or through βAPP- and β-secretase-independent mechanisms.[3] Once released, the β-peptide may remain in solution either as a random coil or as a α-helical structure.[4–6] The transition of the α-helix to β-sheet conformation with concomitant peptide aggregation is one of the proposed mechanisms of oligomer and fibril formation. Moreover, the amyloidogenic mechanism is still a matter of debate, although the outcomes of clinical studies on β-secretase inhibitors strongly suggested that different mechanisms might be involved in familial and sporadic forms of the disease. Recent studies highlighted that neurotoxicity elicited by Aβ assembly would be due to oligomeric species rather than mature fibrils.[7,8] Many different mechanisms of toxicity of Aβ oligomers have been proposed, including membrane interaction and consequent disruption of Ca^{2+} homeostasis,[9,10] or receptor mediated mechanisms, through *N*-methyl-D-aspartate (NMDA)[11–13] and α-amino-3-hydroxy-5-methyl-4-isoxazolepropionic acid (AMPA).[11,14] Consequently, the inhibition of the early stages of Aβ aggregation and the disaggregation of Aβ oligomers and fibrils have been the subject of many studies over the last two decades as a possible approach to treat AD. Among the proposed β-sheet breakers, peptide-based inhibitors called β-sheet breaker peptides (BSBPs),[15] represent a major part of

[a] *Department of Pharmacy, University of Napoli Federico II, Via Domenico Montesano 49, I-80131 Napoli, Italy*
[b] *Net4Science Academic Spin-Off, University "Magna Græcia" of Catanzaro, Viale Europa, 88100 Catanzaro, Italy*
[c] *Institute of Organic Chemistry and Biochemistry of the Czech Academy of Sciences, Flemingovo náměstí 542/2, CZ-16610 Prague, Czech Republic*
[d] *Department of Chemical Sciences, University of Napoli Federico II, Via Cintia 4, I-80126, Napoli, Italy*
[e] *Department of Environmental, Biological and Pharmaceutical Sciences and Technologies, University of Campania "Luigi Vanvitelli", Viale Abramo Lincoln 5, I-81100 Caserta, Italy*
[f] *Istituto Nazionale di Biostrutture e Biosistemi (INBB), Viale delle Medaglie d'Oro 305, I-80145 Roma, Italy*
[g] *Department of Sciences, University of Basilicata, Viale dell'Ateneo Lucano, I-85100 Potenza, Italy. E-mail: mauro.denisco@unibas.it*

† Electronic supplementary information (ESI) available: Fig. S1–S32, Tables S1–S5, Texts S1–S3. See DOI: https://doi.org/10.1039/d4md00057a

‡ F. M., and I. V. have contributed equally to this work and share the first authorship.

the efforts. BSBPs were initially designed by mimicking the hydrophobic core of the amyloidogenic sequence $A\beta_{17-23}$ LVFFAED, involved in the aggregation process.[16] Since the synthesis of the first peptide fragment, by reproducing the hydrophobic core region of $A\beta_{17-21}$ LVFFA,[17] many other BSBPs were proposed, allowing for the identification of key features for the inhibition of the formation and/or disruption of amyloid fibrils. Moreover, mutagenesis experimental studies revealed that the replacement of any residue of $A\beta_{17-23}$ LVFFAED with a proline residue led to a complete loss of fibril formation, while alanine substitutions at residues 17, 18, and 20 did not have an effect on fibril formation, and the replacement of F_{19} reduced fibril formation to 15%.[18]

Indeed, a pentapeptide was designed and synthesized by replacing $V_{18}P$ and $A_{21}D$ to achieve the peptide $A\beta_{17-21}$ LPFFD (also known as iAβ5), which was able to inhibit and disassemble amyloid fibrils *in vitro*.[15,19,20] Then, to minimize exopeptidase cleavage, *N*-terminal and *C*-terminal protections were added, leading to the peptide Ac-LPFFD-NH_2 (iAβ5p, **1**), demonstrating that *N*-terminal acetylation and *C*-terminal amidation enhanced stability in both human plasma and cerebrospinal fluid (CSF).[21–23] However, despite the reduced *in vivo* amyloid deposition, it showed a relatively short *in vivo* half-life. For this reason, the incorporation of *N*-methyl amino acids was subsequently introduced at the cleavage sites of the iAβ5p to prevent endoproteolytic degradation.[22–27] Moreover, the replacement of amide protons involved in β-sheet hydrogen bonding interactions could break the peptide–peptide interactions that promote Aβ fibrillogenesis and prevent the β-sheet formation due to the steric hindrance of the methyl group.[28] Following this approach, a series of iAβ5p peptide analogues were designed,[21] also demonstrating that *N*-methylamino acids increase the stability to the denaturation due to heat, changes in pH (from 2.5 to 10.5), or denaturants such as urea and guanidine-HCl. Furthermore, all *N*-methyl (NMe) containing iAβ5p derivatives, despite their hydrophobic composition, were highly water soluble and this double nature allowed their spontaneous crossing through both synthetic phospholipid bilayer vesicles and cell membranes.[21] Finally, the key role of lysine residue to bind nucleophilic sites mimicking the K_{16} or K_{28} that belong to the middle region of $A\beta_{42}$, K_{16}LVFFAEDVGSNK$_{28}$, was assessed.[29] As it is known, the interactions of K_{16} contribute to the stability of the $A\beta_{42}$ β-sheet, whereas the turn is stabilized by a salt-bridge between the side chain of D_{23} and K_{28}. Moreover, the K_{16} is adjacent to the central hydrophobic cluster (CHC, residues 17–21), the key region in Aβ fibrillogenesis. K_{16} has also been reported to be involved in salt-bridges in certain fibrillar structures of Aβ, whereas other studies suggested that it was predominantly exposed to the solvent and thus available for interaction with other monomers, cell membranes, or potential inhibitors. In a typical drug-discovery process, the knowledge of key drug-target interactions is crucial for the development of new promising drugs.[30,31] This is true also in a peptide drug-discovery process since peptides are often designed based on the structure information of the hot-spots.[32] In the case of development of new BSBPs, the absence of experimental (X-ray or NMR) data about their binding mode on the β-amyloid probably hampers the design of novel BSBPs. Several previous structure–activity relationships (SAR) studies have been undertaken but none consider the putative binding mode of BSBPs.[33–37] In such cases, the design of novel BSBPs can be performed taking into account only the structural features of each peptide (peptide-based design).

With this in mind, starting from the *N*-methyl analogs peptides published by Adessi *et al.*,[21] seven new sequences of BSPBs (**2–8**) were designed (Fig. 1), synthesized and evaluated for their BSB properties through thioflavin binding assays, cellular toxicity and cell-permeable assays. Furthermore, a 3D GRID peptide-based pharmacophore Virtual Screening approach, combined with metadynamics-based enhanced sampling method, was performed to validate and rationalize the outcomes. Globally, our combined approaches were useful to identify peptides **2** and **3** (Fig. 1) as the two most promising BSBPs with a significant improvement of the fibrillogenesis inhibition with respect to the reference peptide iAβ5p (**1**).

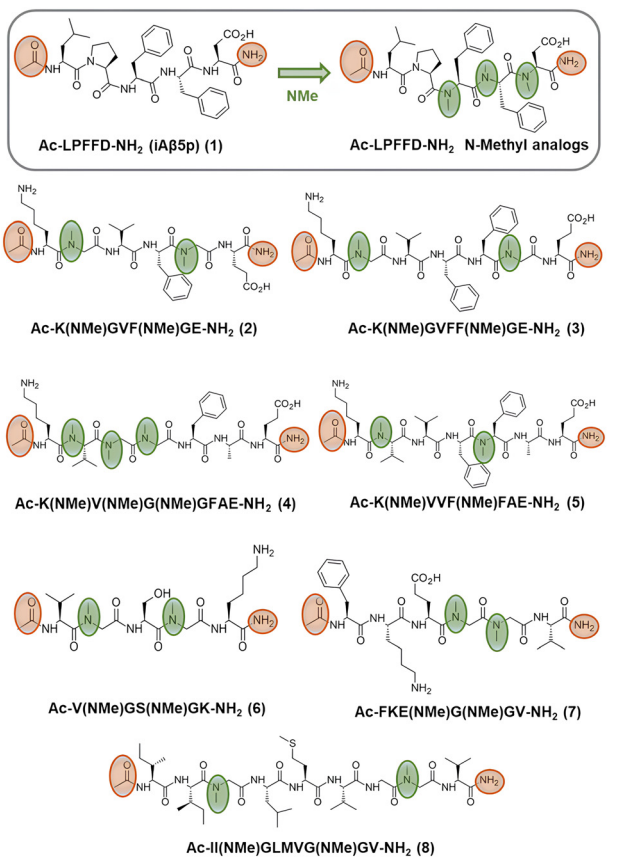

Fig. 1 Two-dimensional structures of parent BSBP iAβ5p (**1**) and the designed peptides library (**2–8**). NMe in round brackets highlight *N*-methylated residues. *N*-Terminal and *C*-terminal end-protection groups are highlighted with orange circles, while *N*-methyl groups are displayed with green circles.

Results and discussion

Peptide design and synthesis

Taking into account the literature information of key features of BSBPs, a library of seven peptides (Fig. 1) was designed with the following features: i) both the *N*-terminal end-protection with the acetyl group and *C*-terminal end-protection with amide group to improve the stability of the peptides in human plasma;[22] ii) the presence of at least one *N*-methyl amino acid residue, to reduce the risk of auto-aggregation of the peptides,[38] and of proteolytic degradation.[27] Furthermore, in addition to the above-mentioned modifications, starting from the well-known iAβ5 ($_{17}$LPFFD$_{21}$), we explored further chemical additions like: iii) replacing P_{18} with (NMe)G_{18} or (NMe)V_{18}; iv) replacing D_{21} with A_{21} and E_{22} of the original Aβ$_{17-22}$ ($_{17}$LVFFAE$_{22}$) fibril sequence; v) replacing in the latter sequence A_{21} with hydrophobic (NMe)G_{21}; vi) replacing L_{17} with K_{17} in order to introduce a positive charge and to also offer a different degree of lipophilia, which is a key element found in known BSBPs. The designed peptides were first synthesized based on Fmoc chemistry. The reactions were carried out in DMF using HOBt/HBTU as an activating species and *N*-methylmorpholine as a protonic scavenger. All peptide couplings and Fmoc deprotection were carried out at room temperature. Under the conditions mentioned above, peptides **2–8** were isolated in poor yields. Since microwave (MW)-assisted organic synthesis is based on the empirical observation that some reactions proceed faster and result in higher yields under microwave irradiation than under conventional heating, it is advantageously applied. Therefore, the reactions (coupling and removal of Fmoc) were carried out in a microwave reactor, and a continuous input power of 450 W (80 °C) and a reaction time of 8 min were applied. The results (Table 1) show that the simple and convenient synthetic procedure allowed us to obtain the peptides with high yields, very short reaction times and, above all, drastically reduced production of sub-products. Interestingly, peptides **4**, **5** and **8** gave the corresponding desired product, which could not be obtained at all by the classical synthetic procedure. All the evidence suggests that under MW irradiation, the reaction proceeds by the same route as under conventional heating and that MW probably aids in the crucial step of inserting the *N*-methyl moiety.

The absence of racemization was investigated by UHPLC-HR MS; the presence of only one peak in the chromatogram of the synthesized peptides suggested the absence of diastereomeric compounds. TOF-MS/MS spectrometric features of the synthesized peptides are reported in Fig. S1–S8, ESI.† It is noteworthy that the higher anti aggregation activity of **2** led to the need for its scramble peptide. Therefore, sequence **7** was designed. The scrambled peptide is obtained through the permutation of the original sequence, and it is finalized to be a negative control to assess that it is not specific sequence-dependent.

Unfortunately, compounds **4**, **5** and **6** were excluded from biological assays due to their low solubility.

Table 1 iAβ5p and analogs yields following MW-assisted organic synthesis

Peptide	Sequence[a]	Yield[b] (%)
1 (iAβ5p)	Ac-LPFFD-NH_2	55
2	Ac-K(NMe)GVF(NMe)GE-NH_2	42
3	Ac-K(NMe)GVFF(NMe)GE-NH_2	68
4	Ac-K(NMe)V(NMe)G(NMe)GFAE-NH_2	30
5	Ac-K(NMe)VVF(NMe)FAE-NH_2	36
6	Ac-V(NMe)GS(NMe)GK-NH_2	41
7	Ac-FKE(NMe)G(NMe)GV-NH_2	40
8	Ac-II(NMe)GLMVG(NMe)GV-NH_2	26

[a] All the molecules were synthesized on Rink Amide MBHA resin after detachment from the resin. [b] Phenomenex Luna RP-C18 column (50 × 2 mm; 3 μm). 1.2 mL min^{-1}. Eluent A = H_2O-0.1% formic acid. Eluent B = MeCN-0.1% formic acid. Gradient: linear 5–95% B in 10 min.

In vitro activity of the synthesized BSBP derivatives

In order to evaluate whether synthesized BSBPs were able to inhibit amyloid fibrils formation, the kinetics of Aβ peptide fibril formation was analyzed by thioflavin T (ThT) assays in the absence or presence of the peptides under test. Indeed, as previously described,[39] ThT presents a typical shift of fluorescence emission maximum from 440 to 482 nm upon specific binding to amyloid fibrils. Aβ$_{1-42}$ peptide (20 μM) was incubated in the presence of the ThT probe, alone or in the presence of BSBP peptides (1 : 10 molar ratio). Indeed, experiments were firstly set up by testing Aβ peptide alone at increasing concentrations (0.6–20 μM). Since 20 μM concentration allowed to obtain a classical typical S-shaped curve with a mid-point at about 400 min (Fig. 2), this was selected as the condition to perform inhibitory experiments by ThT assays. Having been previously reported that β-sheet

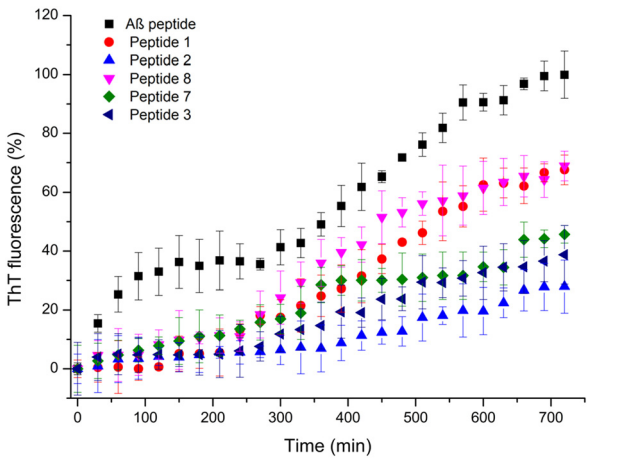

Fig. 2 *In situ* real-time ThT fluorescence assays of Aβ alone (black symbols) and upon incubation with BSBP peptides (ten-fold molar excess). In all the cases, the reported data is derived from three independent experiments.

breakers targeting Aβ fibrils are effective at a molar excess of 10,[40] peptides under study were tested at a concentration of 200 μM. The increase in ThT emission fluorescence at 482 nm was measured over time (12 hours). Interestingly, when the Aβ peptide was incubated with peptides **2** and **3**, a significant reduction of ThT fluorescence emission was observed (Fig. 2), thus indicating a strong inhibition of Aβ peptide fibrillogenesis. This effect was found to be even more pronounced than that exerted by **1** used as a positive control. A comparable effect of peptides **8** and **1** was observed. It has to be noted that also in the presence of scrambled sequence **7**, a significant reduction of ThT fluorescence emission was found, thus indicating that peptide **2** is able to inhibit fibrillogenesis in a sequence-independent manner. Based on these promising results, we decided to analyze the cytotoxic activity of peptides **2** and **3**.

Peptides 2 and 3 do not induce cytotoxic effects

As amyloid fibrils are observed to cause cytotoxicity in cells,[41] with different mechanisms involving cellular membrane destabilization and reactive oxygen species overproduction,[42] the cytotoxic potential of the synthesized iAβ5p (**1**) sequence and peptides **2** and **3** was preliminarily evaluated towards SH-SY5Y cells, which are commonly utilized in several areas of neuroscience, including research on AD.[43] To this purpose, MTT test, which allows the redox mitochondrial activity, and thus the cell viability, to be assessed was employed.[44] When the cells were treated with the three peptides, it was observed that an increase in mitochondrial redox activity occurred in respect to untreated cells used as the control. In fact, setting the viability of untreated control cells equal to 100%, it was observed that all the three peptides were able to induce a weak increase in cell viability, which appeared to be for both **1** and **3** samples independent of the tested dose, whereas peptide **2**-induced mitochondrial redox activity increase was higher as a higher dose was tested (Fig. 3). Thus, the three peptides appeared to be not toxic in the concentration range considered.

Peptides 2 and 3 counteract *in vitro* β-amyloid cytotoxicity and are cell permeable

HR-MS/MS-based cell metabolomic approach on the pellets of the peptides-treated SH-SY5Y cells allowed us to observe that peptides were uptaken within the cells. Representative total ion current (TIC) chromatograms of treated and untreated cells are reported in Fig. S9 of the ESI.† In Fig. 4 (panels B.i, and B.ii), the chromatographic profile of peptides **2** and **3** as pure compounds and that extracted from cell pellets are representatively reported. The chromatographic profile and TOF-MS/MS data of the synthesized peptides (Fig. 4A and S2 and S3, ESI†) are compared with the extracted ion chromatograms from the TOF-MS spectra of the pellet extracts obtained after applying quenching and extraction procedure on the treated cells (Fig. 4B) and their relative TOF-MS/MS spectra (Fig. 4C). This was in line with previous studies showing that the iAβ5p oligopeptide (**1**) was able, beyond inhibiting the formation of amyloid fibrils *in vitro* and to favor their disassembly, to cross the blood–brain barrier.[45] Thus, based on this latter evidence and taking into account the effect of the peptides newly synthesized on cell viability and also the ability of other β-sheet breakers to reverse β-amyloid-induced cytotoxicity,[46] the potential beneficial effect of peptides **2** and **3** was experienced in an *in vitro* system utilizing the functional domain of the β-amyloid peptide. In this context, as the cellular reduction of MTT represents a specific indicator of the initial events underlying the mechanism of β-amyloid peptide toxicity, the MTT test was first carried out exposing SH-SY5Y cells at increasing β-amyloid concentrations. To this purpose, the $A\beta_{25-35}$ fragment was utilized. This 11-mer peptide fragment,

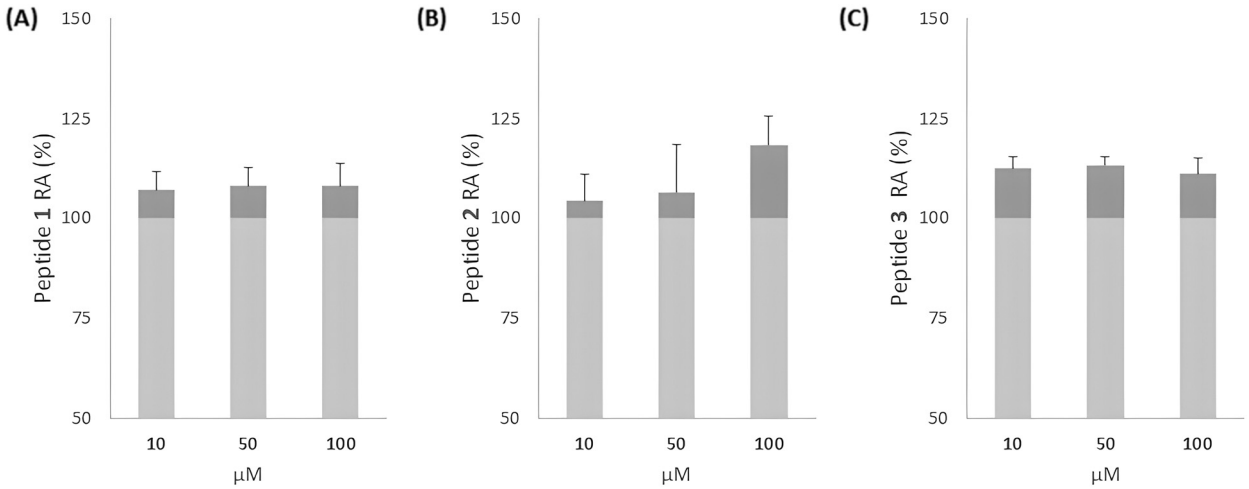

Fig. 3 Cell viability is expressed as the percentage of mitochondrial redox activity of the cells treated with the three peptides (A for peptide **1**, B for peptide **2**, and C for peptide **3**) compared to the untreated control. The values are the mean ± SD of six measurements, carried out in three independent experiments.

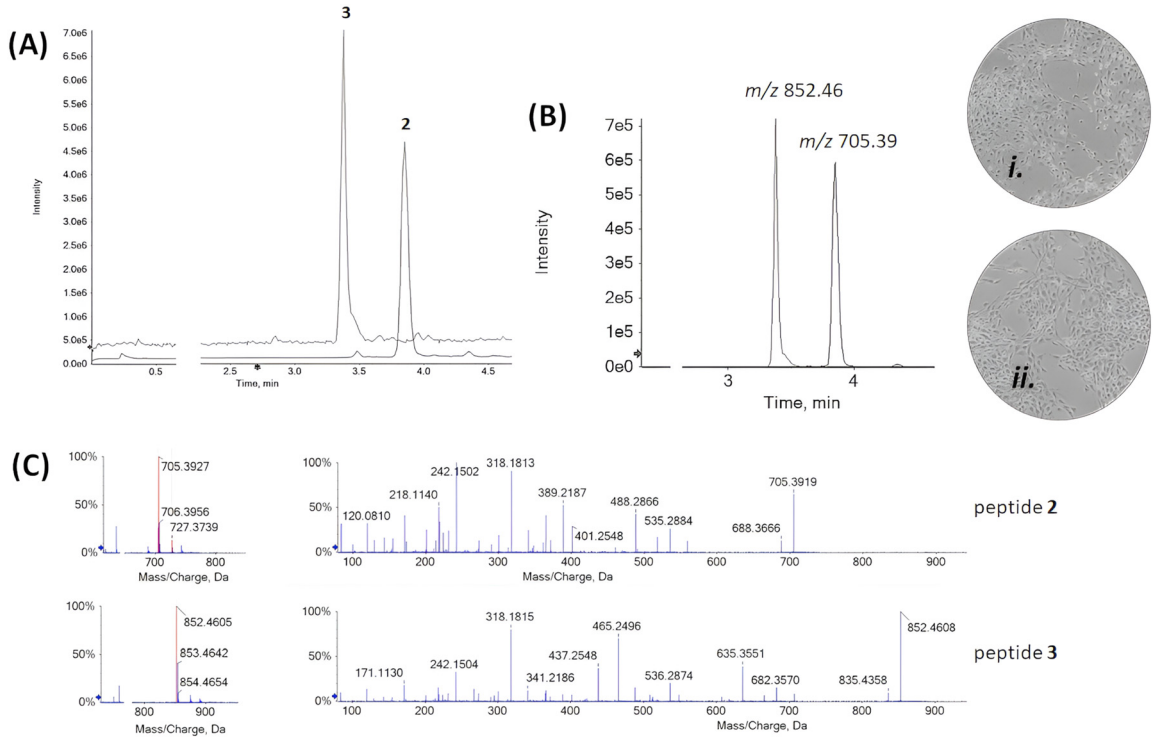

Fig. 4 (A) Total ion current chromatograms of pure peptides **2** and **3**; (B) XIC (extracted ion chromatogram) of the protonated molecular ions at *m/z* 705.39 (peptide **2**) and at *m/z* 852.46 (peptide **3**); (B.i) representative images of peptide **2**-treated cells; (B.ii) representative images of peptide **3**-treated cells; (C) TOF-MS and TOF-MS/MS spectra of peptides **2** and **3** detected in cell pellets (in line with those of pure peptides in Fig. S2 and S3, ESI†).

like its full-length peptide $A\beta_{1-42}$, has shown neurotoxic activities in cultured cells and represents an apparent functional domain of the full-length Aβ responsible for its amyloidogenic and cytotoxic properties.[47] In particular, it is composed of APP regions embedded in the membrane (29–35) and exposed to the membrane–water interface (29–35), and *in vivo* $A\beta_{25-35}$ is localized in neurons of the subiculum and entorhinal cortex. The cytotoxic screening on $A\beta_{25-35}$ highlighted that its 100 μM concentration exerted toxic effects by 50%; further experimentations aimed at assessing the ability of the synthesized peptides to retrieve the Aβ-mediated oxidative damage. Accordingly, cells were treated first with a toxic dose of the $A\beta_{25-35}$ fragment and then with the investigated peptides. MTT data suggested that all the three compounds were differently able to reverse the cell responsiveness to the amyloid fragment oxidant action (Fig. 5). Peptides **1** and **3** notably appeared to exert an inhibitory activity comparable to that induced by the only $A\beta_{25-35}$ domain, whereas a dose-dependent ability to recover the Aβ-induced damage was observed as the peptides' concentration increased. Considering the increase in viability in respect to $A\beta_{25-35}$ treated cells, it was estimated that at the highest tested concentration (100 mM), peptides **1** and **3** augmented the mitochondrial activity by 110.8% and 142.1%, respectively. It is noteworthy that peptide **2** exerted a recovery efficacy already at the 10 μM dose with an increase in viability of about 30% compared to that from cells only Aβ-treated. Also in this case, the efficacy seemed to increase, albeit weakly, with the increase in concentration.

Pharmacophore-based virtual screening (PBVS)

In order to study the molecular basis of peptides **2** and **3** inhibitory activity, we built a 3D GRID-based pharmacophore on 23 known BSBPs data set collected from literature[21] (Table S1, ESI†). We used the FLAP (fingerprints for ligands and proteins) software ver. 2.2.1,[48] which has been already successfully used in the field of peptide-based pharmacophores.[49] GRID-based pharmacophores have been also widely adopted when NMR or X-ray macromolecular complexes are available.[50,51] Unlike the classical pharmacophore approach, the FLAP pharmacophore algorithm (named as FLAPpharm)[52] first aligns molecules using the GRID molecular interaction fields (MIFs),[53] then extracts the common chemical features from this alignment on the basis of the optimal MIFs similarity (called PIFs) and the common atom-centered pharmacophoric pseudo-fields (called pseudoPIFs).[52,54] The pharmacophore hypothesis generation is strongly dependent on the choice of the training set. Here, the global BSBPs library of 23 iAβ5p analogs[21] (Table S1, ESI†) was divided into three groups according to the reported thioflavin (ThT) binding assay[21] expressed as percentage of inhibition (PI) (Fig. S10, ESI†), in ten actives (PI ~60–100%), seven inactives (PI ≤ 20%) and six decoy peptides (PI ~30–50%) (Table S1 and Fig. S10, ESI†).

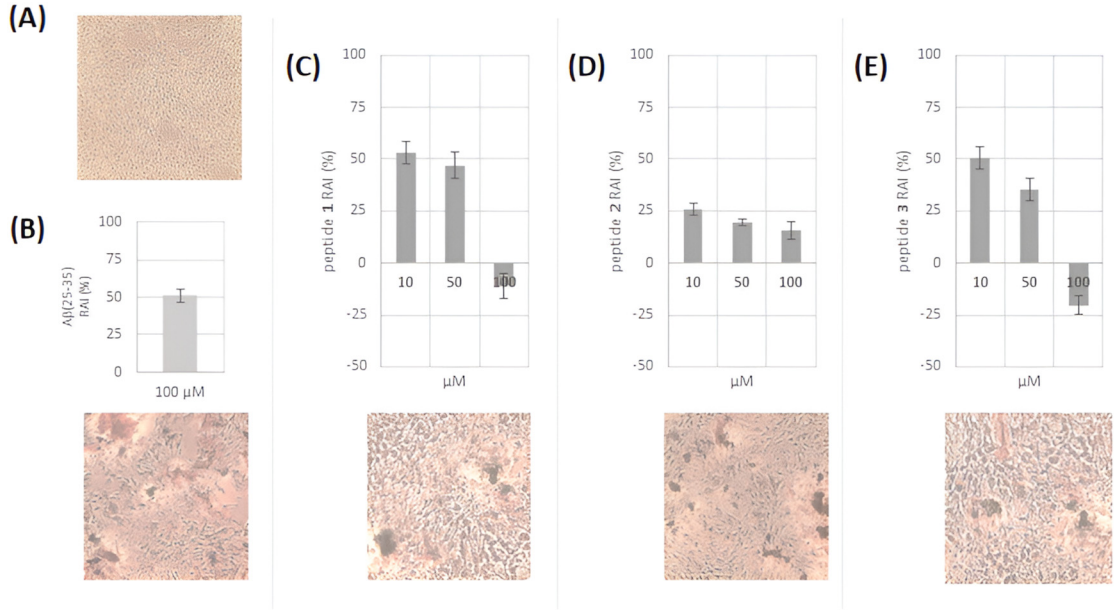

Fig. 5 Cell viability inhibition of SH-SY5Y cells, pre-treated for 24 hours with $A\beta_{25-35}$ at 100 μM concentration level (B) and then exposed to peptides **1**–**3** (C–E). The percentage of the inhibition of mitochondrial redox activity (RAI, %) of the cells was in reference to the control cells, which did not undergo any treatment. Negative values are in line with no inhibition occurrence. The values are the mean ± SD of six measurements, carried out in three independent experiments. Representative images of cells acquired by the inverted phase contrast bright field Zeiss Primovert microscope are reported. (A) Untreated control cells and other relative RAI graph (B) $A\beta_{25-35}$-treated cells; (C) $A\beta_{25-35}$ and peptide **1** treated cells; (D) $A\beta_{25-35}$ and peptide **2** treated cells; (E) $A\beta_{25-35}$ and peptide **3** treated cells.

Specifically, the active and inactive peptides represent our Training set, while the decoys were screened as the test set. The peptide-based pharmacophore hypotheses generated (Text S1, ESI†) led to two different pharmacophore pseudomolecules: Model1 and Model2 (Fig. 6A and B, respectively). The AUC (area under the curve) validation procedure of the two pseudomolecules (Text S2 and Fig. S11 and S12, ESI†) indicated a good discrimination power between active and inactive BSBPs of the H*O descriptor for Model1 (AUC: 86%) and the H*O*DRY descriptor (AUC: 91%) for Model2, as demonstrated also by the good and bad alignment respectively of the active and inactive BSBPs (Fig. S13A and B, ESI†), further supporting both our pharmacophore models that were then used to screen a library of designed *N*-methylated peptides. Both the two PIFs pseudomolecules share a larger hydrogen-bond donor (HBD)

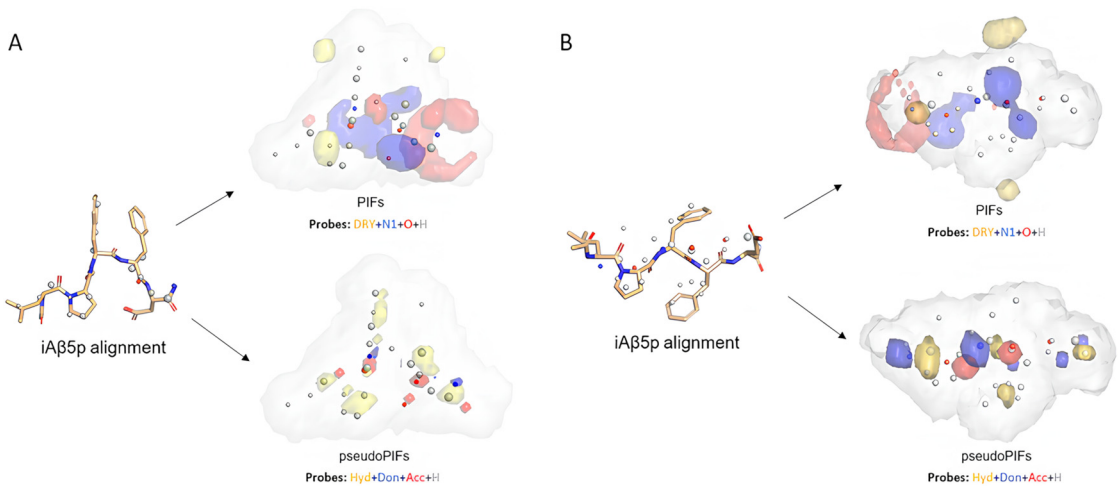

Fig. 6 Pharmacophore pseudomolecules generated by FLAPpharm from the training set alignment. (A) Model1 (*S*-score: 0.667) extracted as common pharmacophoric interaction fields (PIFs) and common pharmacophoric pseudofields (pseudoPIFs). (B) Model2 (*S*-score: 0.517) extracted as common pharmacophoric interaction fields (PIFs) and common pharmacophoric pseudofields (pseudoPIFs). Hydrophobic fields (DRY) are displayed in yellow, hydrogen bond donor fields (N1) are shown in blue, hydrogen-bond acceptor fields (O) are represented in red, while the shape (H) probe is shown as a white solid transparent surface area.

and acceptor (HBA) areas and the three smaller hydrophobic regions. However, looking at the superposition between the lead 1Aβ5p peptide and the two PIFs templates (Fig. S14, ESI†), a different folding arrangement of the amino acid residues can be observed. In fact, concerning the Model1 (Fig. 6A), the amino acid residues of iAβ5p well aligned with the PIFs are P_{18}, F_{19} and F_{20}, with their side chain on the hydrophobic (DRY) MIFs and the backbone oxygen and nitrogen atoms with the HBD (N1) and HBA (O) MIFs, respectively. The end-protection group $-NH_2$ is also well aligned with the HBA area given by the O MIF (Fig. S14, ESI†). The same alignment trend can be observed also with some of the most active iAβ5p analogs. Specifically, the same alignment is conserved also for the BSBPs analogs of group A (A1, A7, A5, and A2), the BSBP analog B1 and those of group C (C2 and C3) (Fig. S14, ESI†), thus indicating that the presence of a single *N*-methyl residue (NMe) at F_{19}, two alternate NMe at F_{19}/D_{21} and two (or three) consecutive NMe at F_{19}/F_{20} and $F_{19}/F_{20}/D_{21}$ amino acids as well as the presence of a (NMe)G residue at *N*-term induces a very similar alignment on PIFs of Model1 as the lead iAβ5p. As it concerns the PIFs template of Model2 (Fig. 6B), it can be noted that the more extended conformation of iAβ5p leads to a different alignment degree. Specifically, the most evident difference with respect to PIFs of Model1 is the presence of an extended HBA area of the O MIF at the *N*-term (instead of *C*-term), aligned with the nitrogen HBD group of residue L_{17}, while it conserved the alignment between the hydrophobic amino acids P_{18}, F_{19} and F_{20} with the DRY MIF, and between the backbone carbonyl oxygen of P_{18}/F_{19} and the HBD area given by the N1 MIF (Fig. S15, ESI†). The same alignment trend is maintained also for iAβ5p analogs of group A (A1, A2, A5, and A7), the analog B1 and those of group C (C2 and C3) (Fig. S15, ESI†). The goodness of validation is also demonstrated by the probe similarity scores of the actives (ranked mostly at the top) and inactives (ranked mostly at the low) BSBPs in both Model1 (Table S2, ESI†) and Model2 (Table S3, ESI†).

FLAPpharm virtual screening of the designed peptides

The designed peptide library **2**–**8** (Fig. 1) was screened using the PIFs pseudomolecule of Model1 and Model2 as template (Fig. 6A and B, respectively). Similarly, in order to better rationalize the rank of the FLAP descriptors, the Test set of decoys (Table S1, ESI†) was also screened. Our analysis was guided by the probe scores, which represent the overlap degree of the MIFs for each probe individually as well as for their combinations. Interestingly, from the ranking of the combined H*O and H*O*DRY descriptors respectively for Model1 (Table S4, ESI†) and Model2 (Table S5, ESI†), the screening results of the decoys in both models resulted in coherence with the previously reported activities, with the most active BSBP iAβ5p ranked at the top, followed by most of the decoys, for which a moderate inhibition activity (IP ~30–50%) is known. The probe scores of our designed peptides fall in a similar range as the decoys set in both Model1 and Model2 (Tables S4 and S5, ESI,† respectively). In particular, peptides **2**, **3**, and **4** have the closest probe values to that of the decoys, while peptide **5** has the lowest probe values. A more detailed picture of the MIFs superposition quality can be observed by analyzing the screening superposition between the N1, O and DRY MIFs of the interesting peptides **2** and **3** against the PIFs templates of Model1 and Model2 (Fig. S16 and S17, ESI,† respectively). Interestingly, analyzing the quality of the superposition between the N1, O and DRY MIFs of the interesting peptides **2** and **3** against the PIFs templates of Model1 and Model2 (Fig. S16 and S17, ESI,† respectively). Interestingly, analyzing the quality of the superposition between the designed peptides and the MIFs of Model1 (Fig. S16, ESI†), it can be observed that a very good overlap not only with the shape (H) probe of the whole peptides **2**, **3** but also between the HBA area is given by the O MIF and the K_{17} of the same peptides. Interestingly, peptides **2** and **3** well overlap K_{17} also with the HBA area of Model2 (Fig. S17, ESI†). This superposition is lost when K_{17} is placed at K_{18} position, as in peptide **4** (Fig. S17, ESI†). On the contrary, the worst-ranked peptide **8** badly overlaps with all the MIFs of both the models. Our results clearly indicate that peptides **2** and **3** well fit to the pharmacophore built on the iAβ5p derivatives series despite the differences in the sequence.

Parallel-tempering in well-tempered ensemble (PT-WTE) simulation of iAβ5p retrieved the pharmacophore Model2 as the most reliable

NMR solution studies of the $Aβ_{1–42}$ sequence revealed that the central hydrophobic core LVFFA can exist in equilibrium between its soluble α-helix form and its aggregated β-sheet conformation, which is neurotoxic.[55,56] Unfortunately, no experimental NMR solution has elucidated the conformation of iAβ5p, to the best of our knowledge. Only previous studies hypothesized that the $V_{18}P$ substitution reduces the propensity of iAβ5p to adopt a β-sheet conformation.[57] In addition, given the good validation results of both the pharmacophores Model1 and Model2, we asked which unbiased conformation of iAβ5p found by FLAPpharm is coherent with the energetically-favored arrangement adopted in explicit water solution. In order to validate the peptide conformer generation found by FLAPpharm, the conformational space of the lead iAβ5p was explored through enhanced sampling PT-WTE simulations. Indeed, the conformational ensembles adopted by linear peptides can be quite vast, making the sampling of the full conformational ensemble a challenge also when using extensive conventional molecular dynamics simulations (MDs). To address this challenge, we used the PT-WTE, which combines parallel-tempering (PT)[58] and well-tempered ensemble (WTE)[59] approaches. In PT-WTE, the sampling is enhanced by enlarging the fluctuations of the potential energy, used as collective variable (CV), with a time-dependent bias potential, thus allowing a great reduction of the number of replicas by

facilitating the replica exchange process. In PT-WTE is possible, in fact, to observe transitions between states that otherwise would be impossible to observe with in standard MonteCarlo (MC) or MDs. A more detailed description of the method is reported in Text S3 of the ESI.† For this work, eight replicas were submitted to PT-WTE simulations at a temperature range from 300 K to 450 K. This protocol is chosen to be similar to that used in previous studies.[60,61] The good ability of each replica to diffuse across all range of temperatures (Fig. S18, ESI†) was further confirmed by the average acceptance probability, which showed that an average of 37% of the exchanges are accepted, deriving from the good overlap between energy distributions at different temperatures (Fig. S19, ESI†). The final free energy surface (FES) was reconstructed by reweighting the bias, according to the Tiwary–Parrinello reweighting algorithm,[62] as a function of two unbiased CVs: the radius of gyration (R_{gyr}), defined on the Cα atoms, and the number of hydrogen bonds (H-bonds) defined on the backbone O atoms (as acceptor groups) and the backbone N atoms (as donor groups). In Fig. 7, the reweighted FES of iAβ5p is shown. This is characterized by a single deep energetic minimum of about −8 kJ mol^{-1} (Fig. 7A), in which the backbone dihedral angles phi and psi of iAβ5p falls into the β-sheet like favored region of the Ramachandran plot (Fig. S20A, ESI†) with no intramolecular H-bond interactions. On the contrary, the conformation of iAβ5p extracted from higher-energy minimum B shows a β-turn arrangement (Fig. 7B), making two intramolecular H-bonds involving carbonyl oxygen of L_{17} and the nitrogen atoms of F_{20} and D_{21}. The formation of such intramolecular H-bonds affects the phi and psi dihedral angles of F_{19} and F_{20} that fall into the allowed regions of the Ramachandran plot (Fig. S20B, ESI†). According to our calculations, the steric hindrance induced by P_{18} influences F_{19} and F_{20} phi and psi backbone dihedrals, thus allowing iAβ5p to adopt a more energetically unstable β-turn conformation of ∼+5 kJ mol^{-1}. A comparison between the PT-WTE conformer of iAβ5p found in basin A with the unbiased conformer retrieved by FLAPpharm in Model2 showed a very good overlap with a RMSD of 0.86 Å calculated on Cα atoms, thus suggesting Model2 as the most reliable since it better resembles the most energetically stable conformation for iAβ5p (Fig. 7C).

PT-WTE simulations of the most promising BSBP 2 and 3

Taking into account the results of the ThT assay (Fig. 2) and the good overlap between the Model2 template PIFs and the H, O, DRY MIFs of the designed peptides, we have selected peptides **2** and **3** to be further investigated with PT-WTE simulation. Thus, the same PT-WTE protocol adopted for the lead BSBPs iAβ5p (**1**) was employed also to further investigate the conformational space of the most promising candidate peptides **2** and **3**. Even for these systems, the eight replicas were able to well diffuse across all ranges of temperatures (Fig. S18B and C, ESI†) with an average of exchanges rate accepted equal to 33% and 28%, respectively, for peptide **2** and peptide **3** and a good overlap between energy distributions at different temperatures (Fig. S19B and C, ESI†). In Fig. 8, the final free energy surface (FES) reconstructed by reweighting the bias is reported, according to the Tiwary–Parrinello reweighting algorithm.[62] The results shown in Fig. 8 clearly demonstrate how the presence of V_{19}, F_{20} and F_{21} is important for the β-sheet formation of peptide **3** extracted from basin A (Fig. 8B), which is slightly more energetically stable than peptide **2** (Fig. 8A). On the contrary, the replacement of F_{21} with (NMe)G_{21} reduces the propensity of peptide **2** to adopt a β-sheet arrangement (Fig. 8A). In addition, peptide **3** can also adopt a quite energetically stable β-turn conformation (∼−1.5 kJ mol^{-1}), as confirmed by the energetic minimum B (Fig. 8B). From the Ramachandran plot reported in Fig. S21–S22 of the ESI,† it can be noted that the

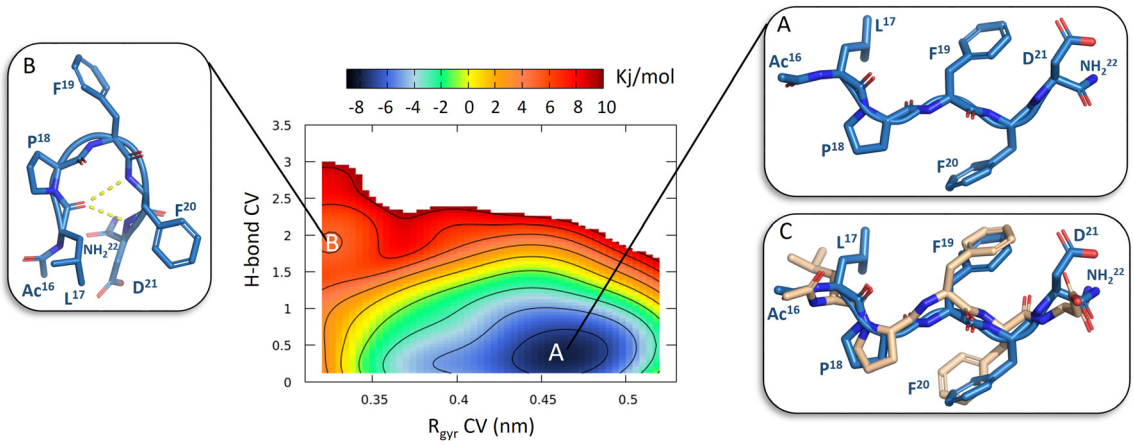

Fig. 7 The reweighted FES of iAβ5p obtained after 150 ns of PT-WTE simulation as a function of R_{gyr} and H-bond CVs. (A) The most representative conformation of iAβ5p extracted from the energetic minimum A, characterized by a β-sheet-like arrangement. (B) The most representative conformation of iAβ5p extracted from the higher energetic minimum B, characterized by β-turn arrangement, with two intramolecular H-bonds displayed as yellow dashed lines. (C) Superposition between the conformation of iAβ5p extracted from the energetic minimum A (blue sticks) and the conformation found by FLAPpharm to build Model2 (wheat sticks) (RMSD: 0.86 Å). Explicit hydrogen atoms are not displayed for clarity reasons.

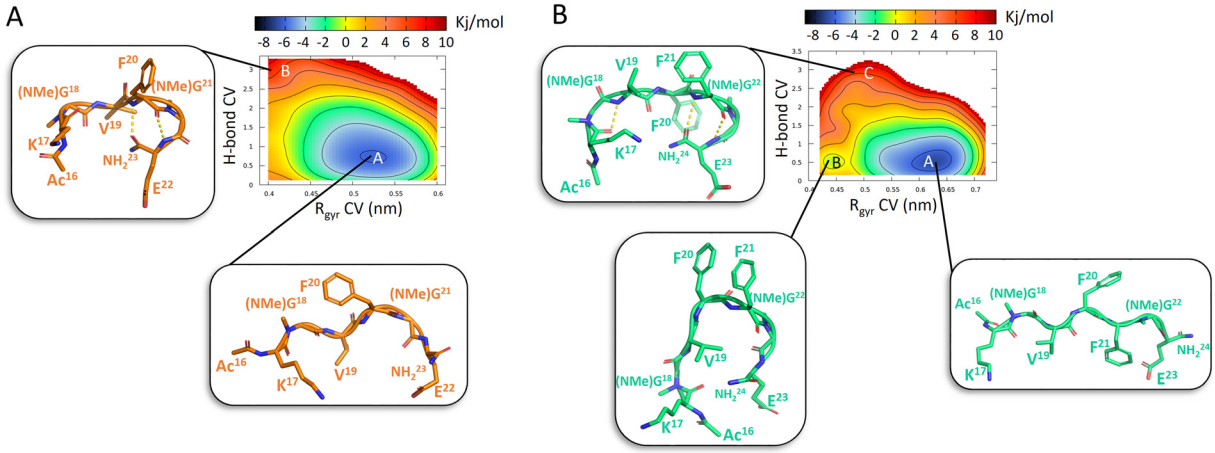

Fig. 8 The reweighted FES of (A) peptide **2** (orange sticks) and (B) peptide **3** (light-green sticks) obtained after 150 ns of PT-WTE simulation as a function of R_{gyr} and H-bond CVs. Hydrogen bond interactions are displayed as yellow dashed lines. Explicit hydrogen atoms are not displayed for clarity reasons.

presence of F_{21} affects the phi/psi dihedral angles of (NMe) G_{22} and E_{23}, thus increasing the propensity of peptide **3** to arrange in the β-turn.

Molecular docking of the predicted energetic minimum conformation of peptide 2 and 3 against the Aβ$_{(1–42)}$ fibrils

The energetic conformation found in basin A of both peptides **2** and **3** (Fig. 8A and B, respectively) were used to verify their binding mode and their affinity toward the Aβ$_{(1–42)}$ fibrils using a blind docking approach. Since amyloid fibrils of the same polypeptide sequence can fold in structurally different morphologies, with a different arrangement of the protofilament conformations,[63] we have used the solution NMR Aβ$_{(1–42)}$ fibrils with U-shaped and S-shaped morphology under the PDB ID: 2BEG and 2NAO, respectively and the LS-shaped Cryo-EM structure of 5OQV (see Materials and methods). Interestingly, blind docking experiments of peptides **2** and **3** retrieved that the most clustered and the lowest binding energy pose binds the region comprised between Q_{15}–V_{24} and L_{34}–V_{40} in most of all the Aβ$_{(1–42)}$ fibrils morphologies (Fig. S27–S32, ESI†). This region was reported as the main interacting region of the fibril.[64] In particular, it was observed that within this region, both peptides **2–3** interacted strongly with the pentameric LS-shaped fibril (PDB ID: 5OQV) with a binding score respectively of −9.13 kcal mol^{-1} and −9.26 kcal mol^{-1} (Fig. S29 and S32, ESI,† respectively). It was further observed that while **2** interacts mostly with the residues of the central hydrophobic region (L_{17}–F_{20}), peptide **3** has the highest affinity for the second hydrophobic region (M_{35}–V_{40}). Compounds that interact with these key residues of these hydrophobic cores have been reported to disrupt the aggregation of fibrils.[65]

Structure activity–relationships

The binding assays revealed that the designed peptides are better Aβ fibrillogenesis inhibitors compared to the parent iAβ5p. The analysis of the overlapping MIFs resulting from the screening of the Model2 advised a key role of the HBA area, suggesting that the nature of the H-bond donor group could play a role in the activity. This information is also confirmed by the results of peptide **7**, in which the HBA area is partially fulfilled with the backbone amide group of V_{22} and accordingly showed a lower activity compared to **2** and **3**.

Conclusions

New β-sheet breaker peptides have been synthesized using the Fmoc chemistry, improved in terms of reduction of reaction times and increase of yields through the application of microwaves. In particular, considering the literature evidence on the key chemical features of BSBPs, a library of seven peptides acetylated at the *N*-terminus and amidated at the *C*-terminus was designed. *N*-Methyl amino acid residues have been introduced since they are known to reduce the risk of self-aggregation of the peptides, and new modifications by substitution of some amino acid residues have been explored to verify the contribution of increased hydrophobicity or the introduction of a positive charge in the bioactivity exercise. The peptides were investigated for their ability to inhibit fibrillogenesis by ThT binding assays, which allowed us to select potentially antiamyloidogenic peptides **2** and **3**. These latter were further proved to be cytoprotective against Aβ toxicity and able to enter in the cell environment. Computational data demonstrated that peptides **2** and **3**, despite the different sequence, shared the same pharmacophoric features of the iAβ5p reference series, and that the pharmacophoric conformations energetically favored both these peptides. PT-WTE metadynamics-based simulations further reinforced the pharmacophore models' predictions by identifying the conformation of peptide iAβ5p from Model2 as the most energetically favored. Finally, docking calculations revealed that peptides **2** and **3** were capable of specifically binding to Aβ$_{(1–42)}$ in their most energetically favored conformations across three

different morphologies, namely, U-shaped, S-shaped, and LS-shaped.

Materials and methods

Materials and instruments for peptide synthesis

All reagents were acquired (Aldrich, Novagel™ and Iris Biotech GmbH) at the highest purity available and used without further purification. The microwave reactor is Milestone microwave reactor, Model Ethos Touch Control Advanced Microwave Labstation, Systems ATC-FO300. The Kaiser Test was utilized to determine if coupling reactions were complete. The ninhydrin used for the Kaiser Test is a solution 0.5 M in methanol. Purification of peptides was performed by semi-preparative HPLC Shimadzu LC-9A using Phenomenex Jupiter-Proteo C18 column (250 × 21.2 mm; 10 μm, 90 Å) and UV detector (λ 254). 0.1% formic acid in water (eluent A) and acetonitrile (eluent B). Gradient: linear 5–95% B in 40 min. Flow rate: 4.0 mL min^{-1}. All solvents used were HPLC grade. The ultra-liquid chromatography-high resolution mass spectrometry (UHPLC-HR MS) analyses were performed by an AB SCIEX Triple TOF 4600 system equipped with a DuoSprayTM plus Shimadzu Nexera UHPLC using Phenomenex Luna C18 column (50 × 2 mm; 3 μm). 0.1% formic acid in water (eluent A) and acetonitrile (eluent B). Gradient: linear 5–95% B in 10 min. Flow rate: 0.5 mL min^{-1}. All solvents used were LC-MS grade. The instrument was controlled by an Analyst® TF 1.7 software, while data was processed using PeakView® software version 2.2. ThT (thioflavin T) fluorescence emission was acquired at 482 nm upon excitation at 450 nm using a SYNERGY H4 microplate reader (Bioteck).

Microwave-assisted solid-phase synthesis: general procedure. Rink amide amino methyl (0.384 g, 0.650 mmol g^{-1}) was put in a manual reaction vessel with a frit column plate, and the outlet was connected to a membrane pump; 2.0 mL DCM was added to the dried resin for resin swelling, stirred gently for 1 min and then the solvent was removed by vacuum filtration; 2.0 mL DMF was added to the resin (washing step), stirred gently for 1 min and then the solvent was removed by vacuum filtration. Deprotection/coupling cycle: 2.5 mL of piperidine 1 M in DMF was added, stirred gently for 3 min in Milestone microwave reactor (T = 80 °C, power = 450 watt); 2.0 mL DCM were added to the resin (washing step), stirred gently for 1 min and then the solvent was removed by vacuum filtration, and washed three times with 2.0 mL DCM, DMF, and diethylether for 1 min, respectively; the Kaiser test was performed. Coupling reaction: 1.25 mmol of Fmoc-AA was dissolved in a solution of 2.5 mL HOBt/HBTU 0.5 M in DMF and 2.5 mL *sym*-collidine 1 M in DMF, the solution was added to the resin and stirred gently for 8 min in Milestone microwave reactor (T = 80 °C, power = 450 watt); the solvent was removed by vacuum filtration, then the resin was washed as previously described here; the cycle "coupling reaction" was repeated for each of the subsequent amino acids according to the sequence using the Fmoc-amino acid derivatives. 2.5 mL of piperidine 1 M in DMF was added, stirred gently for 15 min, and then the solvent was removed by vacuum filtration; resin was washed as previously described here; 2.5 mL of *N*-methyl morpholine 1 M in DMF and 2.5 mL acetic anhydride were added to the resin, stirred gently for 2 min in Milestone microwave reactor (T = 80 °C, power = 450 watt); 2.0 mL DMF were added to the resin (washing step), stirred gently for 1 min and then the solvent was removed by vacuum filtration and 2.5 mL of *N*-methyl morpholine 1 M in DMF and 2.5 mL acetic anhydride were added to the resin, stirred gently for 2 min in Milestone microwave reactor (T = 80 °C, power = 450 watt); the resin was washed as previously described here. Cleavage and purification: 3.0 mL of the cleavage cocktail (TFA/TIS/H_2O 95/2.5/2.5) was added to the dried peptide resin, after 2 hours, 15 mL cold diethyl ether was added dropwise to the filtrate cleavage mixture in a centrifuge tube; after 30 min, the precipitate was isolated by the centrifugation; the crude product was stored for 12 h at −20 °C. Then, after adding 5 mL of H_2O 0.1% TFA, it was lyophilized.

ThT binding assay

ThT (thioflavin T) fluorescence emission was acquired at 482 nm upon excitation at 450 nm using SYNERGY H4 microplate reader (Bioteck). Amyloid β protein fragment 1–42 (20 μM) was incubated alone or in combination with synthetic BSBP peptides (200 μM) in 20 mM Tris-HCl pH 7.4 at 20 °C and ThT (10 μM). *In situ* real-time ThT fluorescence assay was carried out for ∼12 hours, and the fluorescence emission at 482 nm was recorded every 30 min. Fluorescence intensity values at 482 nm were plotted as a function of time.

MTT cytotoxicity assay

The MTT assay was used to determine the metabolic activity on SH-SY5Y human neuroblastoma cells.[66] To this purpose, cells were grown in Dulbecco's modified Eagle medium supplemented with 10% fetal bovine serum, 50.0 U mL^{-1} penicillin, and 100.0 μg mL^{-1} streptomycin, at 37 °C in a humidified atmosphere containing 5% CO_2. Cells were seeded at a density equal to 1.5×10^4 per well, onto 96-well plates, and after 24 h were treated with peptides iAβ5p (**1**), **2**, and **3**. After 48 hours of exposure, cells were treated with MTT (150 μL; 0.50 mg mL^{-1}), previously dissolved in culture media, for 4 h at 37 °C in a 5% CO_2 humidified atmosphere. The MTT solution was then removed, DMSO was added to dissolve formazan, and the absorbance was read at 570 nm using a Victor3 PerkinElmer fluorescence and absorbance reader. The cell viability was expressed as a percentage of mitochondrial redox activity of the cells directly exposed to the synthesized peptides with respect to the unexposed control.

Determination of cytoprotective effect in $A\beta_{25-35}$ induced oxidation cell systems

As it is known that exposure of neuronal cell lines to the β-amyloid peptide causes an increase of neuronal damage

mediated by the induction of ROS synthesis and to evaluate the antioxidant effectiveness of investigated extracts against β-amyloid induced neurotoxicity, the $A\beta_{25-35}$ fragment was used.[66] The $A\beta_{25-35}$ fragment was dissolved in DMSO (12.5 mM, final concentration) and stored at −20 °C until use. SH-5YSY cell lines were seeded in 96-multiwell plates at a density of 2.0×10^4 cells per well, and after 24 h of incubation, were treated with $A\beta_{25-35}$ peptide (100.0 μM) for a further 48 hours exposure time. Then, cells were washed twice with PBS and exposed to peptides **1**, **2**, and **3** (100.0 μM). At the end of exposure time (24 h further), the MTT assay was performed as in the previous paragraph.

UHPLC HR MS-based cell metabolomics

For cell metabolomics, SH-SY5Y cells were seeded at a density of 2.0×10^6 in 100 mm Petri dishes. Countess Automated Cell Counter by Thermo Fisher Scientific Invitrogen was used to provide accurate cell counting. After 24 hours, cells were treated with the synthesized peptides (100 μM) in FBS-free cell culture medium.[67] This latter was instead collected in Falcon® and lyophilized using the FTS-System Flex-dry instrument (SP Scientific, Stone Ridge, NY, USA). Cells were first quenched by the addition of 1 mL of MeOH : H_2O (4 : 1, v : v), and, after collection by physical scraping, extracted using a solution MeOH : H_2O (1 : 1, v : v). Extraction was carried out dipping the tubes with the samples into liquid N_2 for 30 s to snap-freeze the cells and then allowed them to thaw on dry ice. Sample tubes underwent sonication for 5 min in an ultrasound bath. After centrifugation at 3500 rpm and 0 °C for 10 minutes, the supernatant was recovered and lyophilized. The lyophilized supernatants were reconstituted in acetonitrile and subjected to UHPLC-HR MS analyses.

Pharmacophore model generation (FLAPpharm)

The 3D structure of each known BSBPs collected from literature[21] (Table S1, ESI†) was built using the Maestro GUI[68] using the X-ray structure of segment KLVFFA from the $A\beta_{16-21}$ peptide (PDB ID: 2Y2A)[69] as the template. Appropriate structural changes were made to obtain the lead iAβ5p (**1**) and its analogs (Table S1, ESI†) as well as the designed library of *N*-methylated (NMe) peptides (**2**–**8**). Subsequently, each peptide was treated with Protein Preparation Wizard tool[70] to add the missing hydrogen atoms and fix the correct bond order. Training set and decoys set were then imported into the FLAP database performing two levels of stochastic unbiased conformational search: the first level was obtained using the default FLAPpharm parameters by generating 30 conformers for each peptide, while the second level was obtained by increasing the number of peptide unbiased conformers generation up to 100. Then, five 3D GRID Pharmacophores were generated for each level as widely described in the Text S1 of the ESI† with the FLAPpharm algorithm,[52] as implemented in the software FLAP ver.2.2.1.[48]

Molecular dynamics simulations (MDs). iAβ5p (**1**) and peptides **2** and **3** were prepared for MDs using the LEaP module of the AmberTools18 package.[71] The *ff14SB* Amber force field[72] was used to parametrize standard amino acids, while non-canonical amino acids (NCAAs) such as *N*-methylglycine (NMe)G, *N*-methyl-phenylalanine (NMe)F, *N*-methyl-leucine (NMe)L, and *N*-methylaspartic acid (NMe)D were parametrized with the *ffcnaa* Amber force field.[73] Peptides were then solvated in a 10 Å layered cubic water box using the TIP3P water model parameter. Na^+ and Cl^- ions were added to ensure the neutrality of the system and to respect the experimental buffer conditions. Prior to MDs production run, the three systems were firstly minimized with 50 000 steps of steepest descent algorithm, switching to the conjugate gradient algorithm every 1000 steps, and then equilibrated as follows: i) 3 ns of NVT ensemble using the velocity rescaling thermostat by gradually increasing the temperature from 0 K to 300 K, while gradually rescaling the harmonic position restraint force constant on the heavy peptides atoms from 40 to 10 kJ mol^{-1} nm^{-2}; ii) further 5 ns of NVT equilibration at 300 K without any restraint; iii) 5 ns of NPT ensemble at 300 K and 1 atm with the Berendsen barostat without any restraint. Finally, 50 ns of MD production run were performed in NVT ensemble using GROMACS ver. 2018.8.[74]

Metadynamics simulations

PT-WTE. The PLUMED plugin ver. 2.5.3 (ref. 75) was used to perform parallel-tempering in well-tempered ensemble (PT-WTE) simulations. For parallel-tempering, we used eight replicas distributed in a temperature range from 300 K to 450 K, according with the distribution proposed in two previous works.[60,61] Firstly, we have equilibrated each replica with 5 ns of NVT, without any exchange. Subsequently, for the PT-WTE production run, the metadynamics bias potential on the potential energy CV was constructed, depositing every picosecond the Gaussian potential with a Gaussian width of 145 kJ mol^{-1} for peptide **2**, 175 kJ mol^{-1} for peptide **3** and 134 kJ mol^{-1} for the lead iAβ5p (**1**), while the Gaussians height was set up to 2.5 kJ mol^{-1}. Replica exchange was set up every 1 ps. All replicas were simulated in the NVT ensemble for 150 ns.

Well-tempered metadynamics (WT-MetaD). WT-MetaD[76] was used to rescale the Gaussian height by setting up a bias factor equal to 30. Two CVs were chosen to reweight the final FES using the Tiwary–Parrinello algorithm:[62] the first CV is the radius of gyration (R_{gyr}) defined by the Cα of each amino acid (Fig. S23, ESI†), which is able to distinguish between the folded and unfolded states of a protein or a peptide, the second CV is the number of intramolecular hydrogen bonds (H-bonds) calculated considering the backbone O and N atoms as the hydrogen acceptor and donor groups, respectively (Fig. S24, ESI†). For this second CV, the switching functions were set as follows: R_0 = 0.25, NN = 6 and MM = 26.

PT-WTE free energy convergence and block analysis. In order to assess the exhaustiveness of our PT-WTE sampling protocol, we have estimated the free energy convergence and

the error associated to the free-energy as a function of the unbiased R_{gyr} and H-bond CVs used to reweight the FES. The reweighted FES convergence was assessed looking at its evolution over 150 ns simulation time. As reported in Fig. S25 of ESI,† in the last 50 ns of PT-WTE simulation, the FES evolution does not significantly change, thus leading to a final convergence. The error associated with the free-energy was calculated using the so-called block averaging technique.[77] In order to estimate the error bars, the PT-WTE trajectory was split into a set of N blocks (corresponding to the trajectory frames) of equal length. The average error associated with the free energy is shown as a function of increasing block size. As shown in the plot of Fig. S26 of the ESI,† the error is underestimated when small blocks are used. When larger blocks of data are used, the size of the error reaches a plateau value.

Molecular docking. In order to predict the binding affinity of the most promising peptides **2** and **3** against $A\beta_{(1-24)}$ fibrils, blind docking calculations were carried out using AutoDock Vina ver. 1.2.5.[78,79] Firstly, both fibrils and peptides **2–3** were converted into the proper PDBQT format, and the Gasteiger-type charges were added using AutoDock Tools. Secondly, in order to find the region of the $A\beta_{(1-24)}$ fibrils with the best binding affinities, the binding surfaces were defined using extended grid boxes with a grid spacing at 0.375 Å. To include the entire surface of the fibrils, the Grid Boxes were set up with a dimension of: 126 × 72 × 86 Å, 126 × 126 × 126 Å, and 108 × 126 × 102 Å, respectively for the $A\beta_{(1-24)}$ fibrils with the PDB ID: 2BEG,[80] 2NAO[81] and 5OQV.[82] Then, for each peptide, 100 binding poses were generated and energetically evaluated using the specific Vina scoring function. Clusterization of the AutoDock Vina results were performed with the PacDOCK webserver[83] according to the spatial overlapping of the resulting poses, using the complete linkage algorithm. Non-covalent interactions of the best poses between peptides **2–3** and the $A\beta_{(1-24)}$ fibrils (Fig. S27–S32, ESI†) were identified using the Protein-Ligand Interaction Profiler (PLIP) ver. 2.3.0 web service.[84] All the images were rendered using PyMOL ver. 2.0 (**https://pymol.org**).

Author contributions

M. D. N., and D. M. conceived the idea. B. C., M. D. N., F. M., S. Pa., and S. Pe. designed the research. R. G., D. M., F. M., V. P., and I. V. performed the experiments. B. C., M. D. N., R. G., D. M., F. M., and S. Pa. analyzed the data. A. A., B. C., M. D. N., F. M., and S. Pa. drafted the main text of the manuscript. M. D. N., F. M., S. Pa., and S. Pe. contributed to the writing of the manuscript. All authors read and approved the final manuscript.

Conflicts of interest

There are no conflicts to declare.

Acknowledgements

F. M. acknowledges the support from University of Napoli "Federico II" (Grant FRA – Line B – 2020-MoDiGa).

Notes and references

1 M. H. Baig, K. Ahmad, G. Rabbani and I. Choi, *Front. Aging Neurosci.*, 2018, **10**, 21, DOI: **10.3389/fnagi.2018.00021**.
2 T. Iizuka, M. Shoji, T. Kawarabayashi, M. Sato, T. Kobayashi, N. Tada, K. Kasai, E. Matsubara, M. Watanabe, Y. Tomidokoro and S. Hirai, *Biochem. Biophys. Res. Commun.*, 1996, **218**, 238–242, DOI: **10.1006/bbrc.1996.0042**.
3 V. Volloch and S. Rits, *Med. Sci.*, 2018, **6**, 45, DOI: **10.3390/medsci6020045**.
4 D. M. Á. V. Acosta, B. C. Vega, J. C. Basurto, L. G. F. Morales and M. C. R. Hernández, *Int. J. Mol. Sci.*, 2018, **19**, 2415, DOI: **10.3390/ijms19082415**.
5 R. Aleksis, F. Oleskovs, K. Jaudzems, J. Pahnke and H. Biverstål, *Biochimie*, 2017, **140**, 176–192, DOI: **10.1016/j.biochi.2017.07.011**.
6 J. E. Straub and D. Thirumalai, *Annu. Rev. Phys. Chem.*, 2011, **62**, 437–463, DOI: **10.1146/annurev-physchem-032210-103526**.
7 I. Benilova, E. Karran and B. De Strooper, *Nat. Neurosci.*, 2012, **15**, 349–357, DOI: **10.1038/nn.3028**.
8 E. Y. Hayden and D. B. Teplow, *Alzheimer's Res. Ther.*, 2013, **5**, 60, DOI: **10.1186/alzrt226**.
9 S. M. Butterfield and H. A. Lashuel, *Angew. Chem., Int. Ed.*, 2010, **49**, 5628–5654, DOI: **10.1002/anie.200906670**.
10 H. A. Lashuel, D. Hartley, B. M. Petre, T. Walz and P. T. Lansbury, *Nature*, 2002, **418**, 291, DOI: **10.1038/418291a**.
11 G. M. Shankar, B. L. Bloodgood, M. Townsend, D. M. Walsh, D. J. Selkoe and B. L. Sabatini, *J. Neurosci.*, 2007, **27**, 2866–2875, DOI: **10.1523/JNEUROSCI.4970-06.2007**.
12 B. L. Kelly and A. Ferreira, *J. Biol. Chem.*, 2006, **281**, 28079–28089, DOI: **10.1074/jbc.M605081200**.
13 E. M. Snyder, Y. Nong, C. G. Almeida, S. Paul, T. Moran and E. Y. Choi, *Nat. Neurosci.*, 2005, **8**, 1051–1058, DOI: **10.1038/nn1503**.
14 H. Hsieh, J. Boehm, C. Sato, T. Iwatsubo, T. Tomita and S. Sisodia, *Neuron*, 2006, **52**, 831–843, DOI: **10.1016/j.neuron.2006.10.035**.
15 C. Soto, E. M. Sigurdsson, L. Morelli, R. A. Kumar, E. M. Castaño and B. Frangione, *Nat. Med.*, 1998, **4**, 822–826, DOI: **10.1038/nm0798-822**.
16 J. Ghanta, C.-L. Shen, L. L. Kiessling and R. M. Murphy, *J. Biol. Chem.*, 1996, **271**, 29525–29528, DOI: **10.1074/jbc.271.47.29525**.
17 C. Soto, M. S. Kindy, M. Baumann and B. Frangione, *Biochem. Biophys. Res. Commun.*, 1996, **226**, 672–680, DOI: **10.1006/bbrc.1996.1413**.
18 H. Inouye, K. A. Gleason, D. Zhang, S. M. Decatur and D. A. Kirschner, *Proteins*, 2010, **78**, 2306–2321, DOI: **10.1002/prot.22743**.
19 C. Adessi and C. Soto, *Drug Dev. Res.*, 2002, **56**, 184–193, DOI: **10.1002/ddr.10074**.

20 E. M. Sigurdsson, B. Permanne, C. Soto, T. Wisniewski and B. Frangione, *J. Neuropathol. Exp. Neurol.*, 2000, **59**, 11–17, DOI: **10.1093/jnen/59.1.11**.

21 C. Adessi, M. J. Frossard, C. Boissard, S. Fraga, S. Bieler, T. Ruckle, F. Vilbois, S. M. Robinson, M. Mutter, W. A. Banks and C. Soto, *J. Biol. Chem.*, 2003, **278**, 13905–13911, DOI: **10.1074/jbc.m211976200**.

22 S. Bieler and C. Soto, *Curr. Drug Targets*, 2004, **5**, 553–558, DOI: **10.2174/1389450043345290**.

23 P. P. Bose, U. Chatterjee, C. Nerelius, T. Govender, T. Norström, A. Gogoll, A. Sandegren, E. Göthelid, J. Johansson and P. I. Arvidsson, *J. Med. Chem.*, 2009, **52**, 8002–8009, DOI: **10.1021/jm901092h**.

24 H. Amijee, C. Bate, A. Williams, J. Virdee, R. Jeggo, D. Spanswick, D. I. C. Scopes, J. M. Treherne, S. Mazzitelli, R. Chawner, C. E. Eyers and A. J. Doig, *Biochemistry*, 2012, **51**, 8338–8352, DOI: **10.1021/bi300415v**.

25 K. Rajasekhar, S. Suresh, R. Manjithaya and T. Govindaraju, *Sci. Rep.*, 2015, **5**, 8139, DOI: **10.1038/srep08139**.

26 K. Rajasekhar, C. Madhu and T. Govindaraju, *ACS Chem. Neurosci.*, 2016, **7**, 1300–1310, DOI: **10.1021/acschemneuro.6b00175**.

27 M. Mindt, J. M. Risse, H. Gruß, N. Sewald, B. J. Eikmanns and V. F. Wendisch, *Sci. Rep.*, 2018, **8**, 12895, DOI: **10.1038/s41598-018-31309-5**.

28 D. J. Gordon, K. L. Sciarretta and S. C. Meredith, *Biochemistry*, 2001, **40**, 8237–8245, DOI: **10.1021/bi002416v**.

29 S. Sinha, H. J. L. Dahabada and G. Bitan, *ACS Chem. Neurosci.*, 2012, **3**, 473–481, DOI: **10.1021/cn3000247**.

30 A. Deplano, C. M. Morgillo, M. Demurtas, E. Björklund, M. Cipriano, M. Svensson, S. Hashemian, G. Smaldone, E. Pedone, F. J. Luque, M. G. Cabiddu, E. Novellino, C. J. Fowler, B. Catalanotti and V. Onnis, *Eur. J. Med. Chem.*, 2017, **136**, 523–542, DOI: **10.1016/j.ejmech.2017.05.033**.

31 A. Deplano, J. Karlsson, M. Svensson, F. Moraca, B. Catalanotti, C. J. Fowler and V. Onnis, *J. Enzyme Inhib. Med. Chem.*, 2020, **35**, 815–823, DOI: **10.1080/14756366.2020.1743283**.

32 M. J. de Vega, M. Martín-Martínez and R. González-Muñiz, *Curr. Top. Med. Chem.*, 2007, **7**, 33–62, DOI: **10.2174/156802607779318325**.

33 S. Shuaib, S. S. Narang, D. Goyal and B. Goyal, *J. Cell. Biochem.*, 2019, **120**, 17935–17950, DOI: **10.1002/jcb.29061**.

34 M. H. Viet, K. Siposova, Z. Bednarikova, A. Antosova, T. T. Nguyen, Z. Gazova and M. S. Li, *J. Phys. Chem. B*, 2015, **119**, 5145–5155, DOI: **10.1021/acs.jpcb.5b00006**.

35 G. Eskici and M. Gur, *PLoS One*, 2013, **8**, e66178, DOI: **10.1371/journal.pone.0066178**.

36 N. J. Bruce, D. Chen, S. G. Dastidar, G. E. Marks, C. H. Schein and R. A. Bryce, *Peptides*, 2010, **31**, 2100–2108, DOI: **10.1016/j.peptides.2010.07.015**.

37 C. Hetényi, T. Körtvélyesi and B. Penke, *Bioorg. Med. Chem.*, 2002, **10**, 1587–1593, DOI: **10.1016/s0968-0896(01)00424-2**.

38 K. L. Sciarretta, D. J. Gordon and S. C. Meredith, *Methods Enzymol.*, 2006, **413**, 273–312, DOI: **10.1016/s0076-6879(06)13015-3**.

39 R. Gaglione, G. Smaldone, R. Di Girolamo, R. Piccoli, E. Pedone and A. Arciello, *Biochim. Biophys. Acta, Gen. Subj.*, 2018, **1862**, 377–384, DOI: **10.1016/j.bbagen.2017.11.018**.

40 V. Minicozzi, R. Chiaraluce, V. Consalvi, C. Giordano, C. Narcisi, P. Punzi, G. C. Rossi and S. Morante, *J. Biol. Chem.*, 2014, **289**, 11242–11252, DOI: **10.1074/jbc.M113.537472**.

41 C. Pang, N. Zhang and M. Falahati, *Int. J. Biol. Macromol.*, 2021, **169**, 532–540, DOI: **10.1016/j.ijbiomac.2020.12.130**.

42 B. Katebi, M. Mahdavimehr, A. A. Meratan, A. Ghasemi and M. Nemat-Gorgani, *Arch. Biochem. Biophys.*, 2018, **659**, 22–32, DOI: **10.1016/j.abb.2018.09.024**.

43 H. Xicoy, B. Wieringa and G. J. M. Martens, *Mol. Neurodegener.*, 2017, **12**, 10, DOI: **10.1186/s13024-017-0149-0**.

44 M. K. Siddiqi, N. Majid, P. Alam, S. Malik, A. Alam, S. Rajan, M. R. Ajmal and R. H. Khan, *Int. J. Biol. Macromol.*, 2020, **143**, 102–111, DOI: **10.1016/j.ijbiomac.2019.11.222**.

45 A. Francioso, P. Punzi, A. Boffi, C. Lori, S. Martire, C. Giordano, M. D'Erme and L. Mosca, *Bioorg. Med. Chem.*, 2015, **23**, 1671–1683, DOI: **10.1016/j.bmc.2015.02.041**.

46 Y. Nakagami, S. Nishimura, T. Murasugi, I. Kaneko, M. Meguro, S. Marumoto, H. Kogen, K. Koyama and T. Oda, *Br. J. Pharmacol.*, 2002, **137**, 676–682, DOI: **10.1038/sj.bjp.0704911**.

47 G. Shanmugam and P. L. Polavarapu, *Biophys. J.*, 2004, **87**, 622–630, DOI: **10.1529/biophysj.104.040907**.

48 M. Baroni, G. Cruciani, S. Sciabola, F. Perruccio and J. S. Mason, *J. Chem. Inf. Model.*, 2007, **47**, 279–294, DOI: **10.1021/ci600253e**.

49 A. Lupia, S. Mimmi, E. Iaccino, D. Maisano, F. Moraca, C. Talarico, E. Vecchio, G. Fiume, F. Ortuso, G. Scala, I. Quinto and S. Alcaro, *Eur. J. Med. Chem.*, 2020, **185**, 111838, DOI: **10.1016/j.ejmech.2019.111838**.

50 F. Moraca, J. Amato, F. Ortuso, A. Artese, B. Pagano, E. Novellino, S. Alcaro, M. Parrinello and V. Limongelli, *Proc. Natl. Acad. Sci. U. S. A.*, 2017, **114**, E2136–E2145, DOI: **10.1073/pnas.1612627114**.

51 F. Ortuso, T. Langer and S. Alcaro, *Bioinformatics*, 2006, **22**, 1449–1455, DOI: **10.1093/bioinformatics/btl115**.

52 S. Cross, M. Baroni, L. Goracci and G. Cruciani, *J. Chem. Inf. Model.*, 2012, **52**, 2587–2598, DOI: **10.1021/ci300153d**.

53 P. J. Goodford, *J. Med. Chem.*, 1985, **28**, 849–857, DOI: **10.1021/jm00145a002**.

54 S. Cross, F. Ortuso, M. Baroni, G. Costa, S. Distinto, F. Moraca, S. Alcaro and G. Cruciani, *J. Chem. Inf. Model.*, 2012, **52**, 2599–2608, DOI: **10.1021/ci300154n**.

55 S. Tomaselli, V. Esposito, P. Vangone, N. A. J. van Nuland, A. M. J. J. Bonvin, R. Guerrieri, T. Tancredi, P. A. Temussi and D. Picone, *ChemBioChem*, 2006, **7**, 257–267, DOI: **10.1002/cbic.200500223**.

56 T. Lührs, C. Ritter, M. Adrian, D. Riek-Loher, B. Bohrmann, H. Döbeli, D. Schubert and R. Riek, *Proc. Natl. Acad. Sci. U. S. A.*, 2005, **102**, 17342–17347, DOI: **10.1073/pnas.0506723102**.

57 S. J. Wood, R. Wetzel, J. D. Martin and M. R. Hurle, *Biochemistry*, 1995, **34**, 724–730, DOI: **10.1021/bi00003a003**.

58 D. J. Earl and M. W. Deem, *Phys. Chem. Chem. Phys.*, 2005, **7**, 3910–3916, DOI: **10.1039/B509983H**.

59 M. Bonomi and M. Parrinello, *Phys. Rev. Lett.*, 2010, **104**, 190601, DOI: **10.1103/PhysRevLett.104.190601**.
60 F. Palazzesi, A. Barducci, M. Tollinger and M. Parrinello, *Proc. Natl. Acad. Sci. U. S. A.*, 2013, **110**, 14237–14242, DOI: **10.1073/pnas.1313548110**.
61 M. K. Prakash, A. Barducci and M. Parrinello, *J. Chem. Theory Comput.*, 2011, **7**, 2025–2027, DOI: **10.1021/ct200208h**.
62 P. Tiwary and M. A. Parrinello, *J. Phys. Chem. B*, 2015, **119**, 736–742, DOI: **10.1021/jp504920s**.
63 M. Fändrich, J. Meinhardt and N. Grigorieff, Structural polymorphism of Alzheimer Aβ and other fibrils, *Prion*, 2009, **3**, 89–93.
64 S. Boopathi and P. Kolandaivel, Role of the zinc and copper metal ions in amyloid β-peptides Aβ1-40 and Aβ1-42 aggregation, *RSC Adv.*, 2014, **4**, 38951–38965.
65 M. H. Rodríguez, L. G. F. Morales, J. C. Basurto and M. C. R. Hernández, Molecular Docking and Molecular Dynamics Simulation to Evaluate Compounds That Avoid the Amyloid Beta 1-42 Aggregation. In: Roy, K. (eds) Computational Modeling of Drugs Against Alzheimer's Disease, *Neuromethods*, 2018, **132**, DOI: **10.1007/978-1-4939-7404-7_9**.
66 S. Pacifico, M. Gallicchio, P. Lorenz, S. M. Duckstein, N. Potenza, S. Galasso, S. Marciano, A. Fiorentino, F. C. Stintzing and P. Monaco, *Chem. Res. Toxicol.*, 2014, **27**, 611–626, DOI: **10.1021/tx5000415**.
67 A. Ciardiello, S. Altieri, F. Ballarini, V. Bocci, S. Bortolussi, L. Cansolino, D. Carlotti, M. Ciocca, R. Faccini, A. Facoetti, C. Ferrari, L. Ficcadenti, E. Furfaro, S. Giagu, F. Iacoangeli, G. Macioce, C. Mancini-Terracciano, A. Messina, L. Milazzo, S. Pacifico, S. Piccolella, I. Postuma, D. Rotili, V. Vercesi, C. Voena, F. Vulcano and S. Capuani, *Phys. Med.*, 2022, **94**, 75–84, DOI: **10.1016/j.ejmp.2021.12.011**.
68 *Schrödinger Release 2019-1: Maestro*, Schrödinger, LLC, New York, NY.
69 J. P. Colletier, A. Laganowsky, M. Landau, M. Zhao, A. B. Soriaga, L. Goldschmidt, D. Flot, D. Cascio, M. R. Sawaya and D. Eisenberg, *Proc. Natl. Acad. Sci. U. S. A.*, 2011, **108**, 16938–16943, DOI: **10.1073/pnas.1112600108**.
70 G. Madhavi Sastry, M. Adzhigirey, T. Day, R. Annabhimoju and W. Sherman, *J. Comput.-Aided Mol. Des.*, 2013, **27**, 221–234, DOI: **10.1007/s10822-013-9644-8**.
71 D. A. Case, I. Y. Ben-Shalom, S. R. Brozell, D. S. Cerutti, T. E. Cheatham III, V. W. D. Cruzeiro, R. E. Darden, D. Duke, M. K. Ghoreishi, H. Gilson, A. W. Gohlke, D. Goetz, R. Greene, N. Harris, Y. Homeyer, S. Huang, A. Izadi, T. Kovalenko, T. S. Kurtzman, S. Lee, P. LeGrand, C. Li, J. Lin, T. Liu, R. Luchko, D. J. Luo, K. M. Mermelstein, Y. Merz, G. Miao, C. Monard, H. Nguyen, I. Nguyen, A. Omelyan, F. Onufriev, R. Pan, D. R. Qi, A. Roe, C. Roitberg, S. Sagui, J. Schott-Verdugo, C. L. Shen, J. Simmerling, R. Smith, J. Salomon-Ferrer, R. C. Swails, J. Walker, H. Wang, R. M. Wei, X. Wolf, L. Wu, D. M. Y. Xiao and P. A. Kollman, *AMBER 2018*, University of California, San Francisco, 2018.
72 J. A. Maier, C. Martinez, K. Kasavajhala, L. Wickstrom, K. E. Hauser and C. Simmerling, *J. Chem. Theory Comput.*, 2015, **11**, 3696–3713, DOI: **10.1021/acs.jctc.5b00255**.
73 G. A. Khoury, J. Smadbeck, P. Tamamis, A. C. Vandris, C. A. Kieslich, C. A. Floudas and A. C. S. Synth, *Biologia*, 2014, **3**, 855–869, DOI: **10.1021/sb400168u**.
74 D. van der Spoel, E. Lindahl, B. Hess, G. Groenhof, A. E. Mark and H. J. C. Berendsen, *J. Comput. Chem.*, 2020, **26**, 1701–1718, DOI: **10.1002/jcc.20291**.
75 G. A. Tribello, M. Bonomi, D. Branduardi, C. Camilloni and G. Bussi, *Comput. Phys. Commun.*, 2014, **185**, 604–613, DOI: **10.1016/j.cpc.2013.09.018**.
76 A. Barducci, G. Bussi and M. Parrinello, *Phys. Rev. Lett.*, 2008, **100**, 020603, DOI: **10.1103/PhysRevLett.100.020603**.
77 G. Bussi and A. Laio, *Nat. Rev. Phys.*, 2020, **2**, 200–212, DOI: **10.1038/s42254-020-0153-0**.
78 J. Eberhardt, D. Santos-Martins, A. F. Tillack and S. Forli, AutoDock Vina 1.2.0: New Docking Methods, Expanded Force Field, and Python Bindings, *J. Chem. Inf. Model.*, 2021, **61**, 3891–3898, DOI: **10.1021/acs.jcim.1c00203**.
79 O. Trott and A. J. Olson, AutoDock Vina: improving the speed and accuracy of docking with a new scoring function, efficient optimization and multithreading, *J. Comput. Chem.*, 2010, **31**, 455–461, DOI: **10.1002/jcc.21334**.
80 T. Lührs, C. Ritter, M. Adrian, D. Riek-Loher, B. Bohrmann, H. Döbeli, D. Schubert and R. Riek, 3D structure of Alzheimer's amyloid-beta(1-42) fibrils, *Proc. Natl. Acad. Sci. U. S. A.*, 2005, **102**, 17342–17347.
81 M. A. Wälti, F. Ravotti, H. Arai, C. G. Glabe, J. S. Wall, A. Böckmann, P. Güntert, B. H. Meier and R. Riek, Atomic-resolution structure of a disease-relevant Aβ(1-42) amyloid fibril, *Proc. Natl. Acad. Sci. U. S. A.*, 2016, **113**, E4976–E4984.
82 L. Gremer, D. Schölzel, C. Schenk, E. Reinartz, J. Labahn, R. B. G. Ravelli, M. Tusche, C. Lopez-Iglesias, W. Hoyer, H. Heise, D. Willbold and G. F. Schröder, Fibril structure of amyloid-β(1-42) by cryo-electron microscopy, *Science*, 2017, **358**, 116–119.
83 J. Carbone, A. Ghidini, A. Romano, L. Gentilucci and F. Musiani, PackDOCK: A Web Server for Positional Distance-Based and Interaction-based Analysis of Docking Results, *Molecules*, 2022, **27**, 6884.
84 M. F. Adasme, K. L. Linnemann, S. N. Bolz, F. Kaiser, S. Salentin, V. J. Haupt and M. Schroeder, PLIP 2021: expanding the scope of the protein-ligand interaction profiler to DNA and RNA, *Nucleic Acids Res.*, 2021, **49**, W530–W534, DOI: **10.1093/nar/gkab294**.

